ACS OMEGA

http://pubs.acs.org/journal/acsodf

Article

Sandwich-Doping for a Large Schottky Barrier and Long-Term Stability in Graphene/Silicon Schottky Junction Solar Cells

Min Ji Im, Seok-Ki Hyeong, Min Park, Seoung-Ki Lee, Tae-Wook Kim, Gun Young Jung,* and Sukang Bae*

Cite This: *ACS Omega* 2021, 6, 3973−3979

Read Online

ACCESS | Metrics & More | Article Recommendations | Supporting Information

ABSTRACT: Doping is an effective method for controlling the electrical properties and work function of graphene which can improve the power conversion efficiency of graphene-based Schottky junction solar cells (SJSCs). However, in previous approaches, the stability of chemical doping decreased over time due to the decomposition of dopants on the surface of graphene under ambient conditions. Here, we report an efficient and strong p-doping by simple sandwich doping on both the top and bottom surfaces of graphene. We confirmed that the work function of sandwich-doped graphene increased by 0.61 eV and its sheet resistance decreased by 305.8 Ω/sq, compared to those of the pristine graphene. Therefore, the graphene-silicon SJSCs that used sandwich-doped graphene had a power conversion efficiency of 10.02%, which was 334% higher than that (2.998%) of SJSCs that used pristine graphene. The sandwich-doped graphene-based silicon SJSCs had excellent long-term stability over 45 days without additional encapsulation.

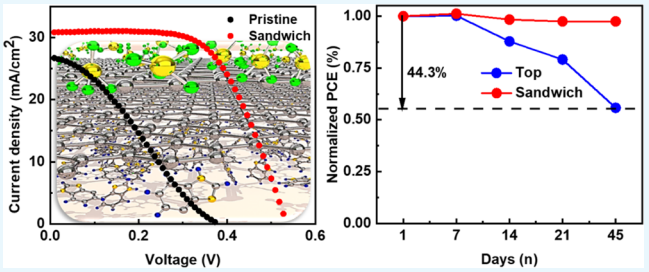

INTRODUCTION

Silicon (Si) solar cells based on the p−n junction have the highest power conversion efficiency (PCE) of 26.6%.[1] However, these solar cells are fabricated by an expensive ion implantation process to substitute dopants into their lattices at high temperature. The high temperature process causes the decrease in Si minority carrier lifetime, thereby degrading the efficiency of Si solar cells. Compared to the traditional p−n junction solar cells, the Schottky junction solar cells (SJSCs) are fabricated at low temperature; this method has the advantage of easy manufacturing at low cost. The Schottky junction induces a low forward voltage drop, while allowing for fast switching speed and a low voltage overshoot when turning lights on.[2−4] Several SJSCs based on the Si semiconductor have used materials with metallic properties as the metal layer such as conducting polymers,[5,6] thin metals,[4,7] metal oxides,[8,9] and two-dimensional materials as the metal layer.[10−12]

Among these materials, graphene is an attractive material for use in SJSCs owing to its high carrier mobility, transparency in visible wavelengths, chemical stability, and electrical properties that can be adjusted easily by doping.[13−15] Graphene also has potential uses as a transparent conductive electrode,[16,17] an additive material to photoactive layers,[18] and a charge transport layer in the field of solar cells.[19,20] It has been first applied to SJSCs as a metal junction layer, as reported by Li et al. in 2010.[21] However, these SJSCs have high charge-carrier recombination rates and a low work function (W_G), so they have a poor PCE of 1.5%.

To improve the PCE of SJSCs, a large Schottky barrier height (ϕ_B) between the p-type graphene and n-type Si should be obtained; this status can be achieved by elevating W_G. Increased ϕ_B reduces the charge-carrier recombination rates and increases the photovoltaic performance. Many efforts to increase the ϕ_B of SJSCs have used postdoping with strong acids[22,23] (e.g., $SOCl_2$, H_2O_2, and HNO_3) and polymer acids[24,25] (e.g., trietylenetetramine (TETA) and trifluoromethanesulfonic acid (TFSA)) on the graphene surface to achieve a high W_G. Cui et al.[22] reported that the PCE of a graphene/Si SJSC can be increased from 2.45 to 5.95% by doping on the surface of graphene with $SOCl_2$. However, this doping effect deteriorated over time to PCE = 2.24% after 8 days under ambient conditions. The highest PCE of the graphene/silicon SJSCs reported so far is 14.5% by chemical doping with HNO_3 combined with TiO_2 antireflection coatings (ARC),[25] but this PCE also deteriorated, in this case, to 6.5% after 20 days. Such a deterioration is the remaining problem to solve.

Dual-side photoinduced doping of graphene with a poly(3-hexylthiophene-2,5-diyl) (P3HT) thin film at the graphene/silicon interface and subsequent TFSA doping for the top

Received: December 2, 2020
Accepted: January 15, 2021
Published: January 26, 2021

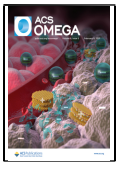

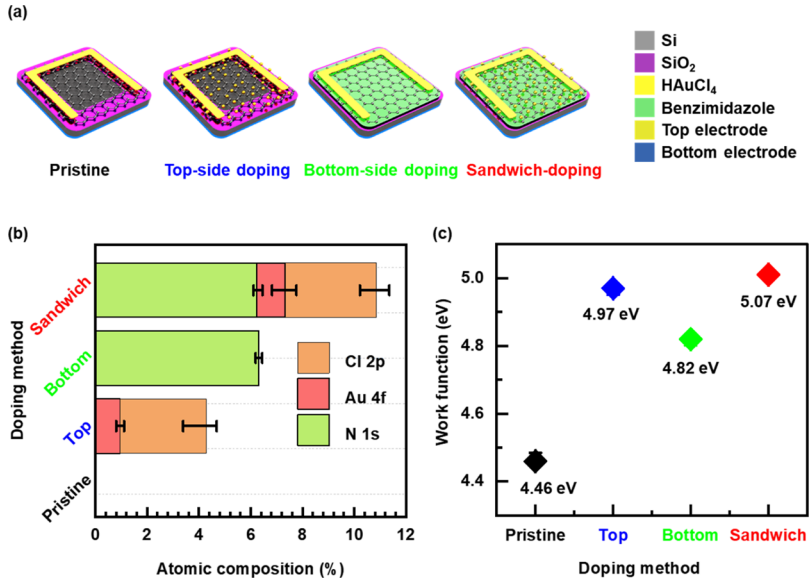

Figure 1. (a) Schematic illustration of the pristine graphene/silicon SJSC, top-side-doped, bottom-side-doped, and sandwich-doped graphene/silicon SJSCs. (b) Atomic compositions of N 1s, Au 4f, and Cl 2p for the four differently doped graphene. (c) Work function by the doping method.

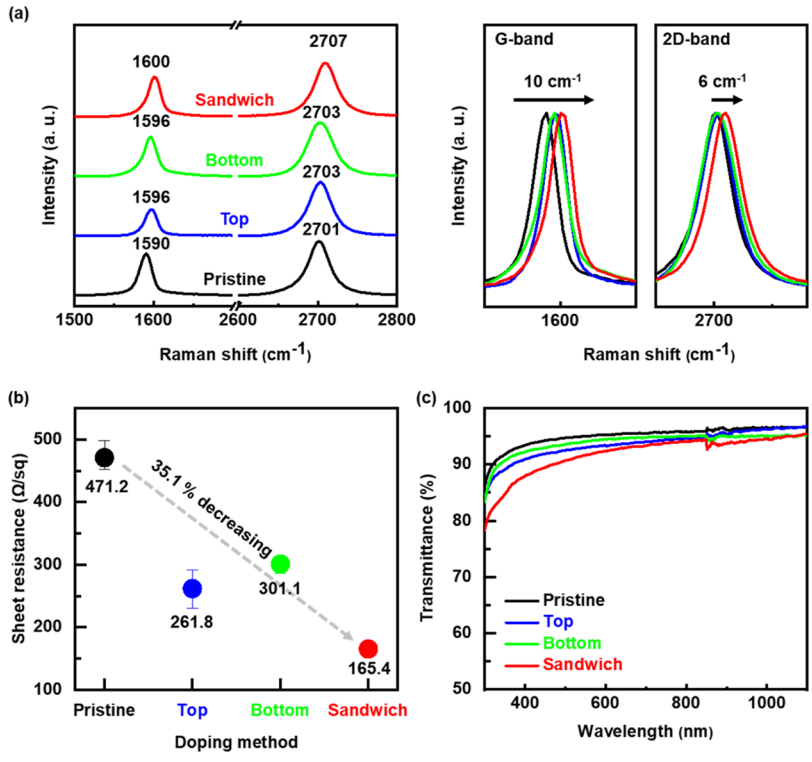

Figure 2. (a) Raman spectra of the graphene transferred onto the SiO_2 substrate (left) and magnified spectra of G- and 2D-band regions (right). (b) Sheet resistance and (c) optical transmittance of the differently doped graphene.

surface of graphene increased the PCE to 10.24% from the pristine (undoped) graphene PCE of 0.6%.[23] However, the dopant is not immediately activated, so the P3HT interlayer must be exposed to sunlight (AM 1.5G) at least for 1 h to saturate the doping effect.

In this study, we developed a simple process that we call sandwich doping for graphene. Sandwich doping is a double-sided chemical-doping process: first, the bottom side of the graphene is doped by adding benzimidazole (BI) during the etching process of copper (Cu) from graphene/Cu foil; then, the bottom-side-doped graphene is transferred to a Si substrate, and the top side of the graphene is doped using $HAuCl_4$ solution. We measured W_G, sheet resistance R_S, and stability of graphene after sandwich doping and compared them to graphene that had been only top-side-doped, only bottom-side-doped, or had not been doped (pristine). The sandwich-doped graphene had the highest W_G, the lowest R_S, and the best photovoltaic performance. The SJSC with the

https://dx.doi.org/10.1021/acsomega.0c05871
ACS Omega 2021, 6, 3973−3979

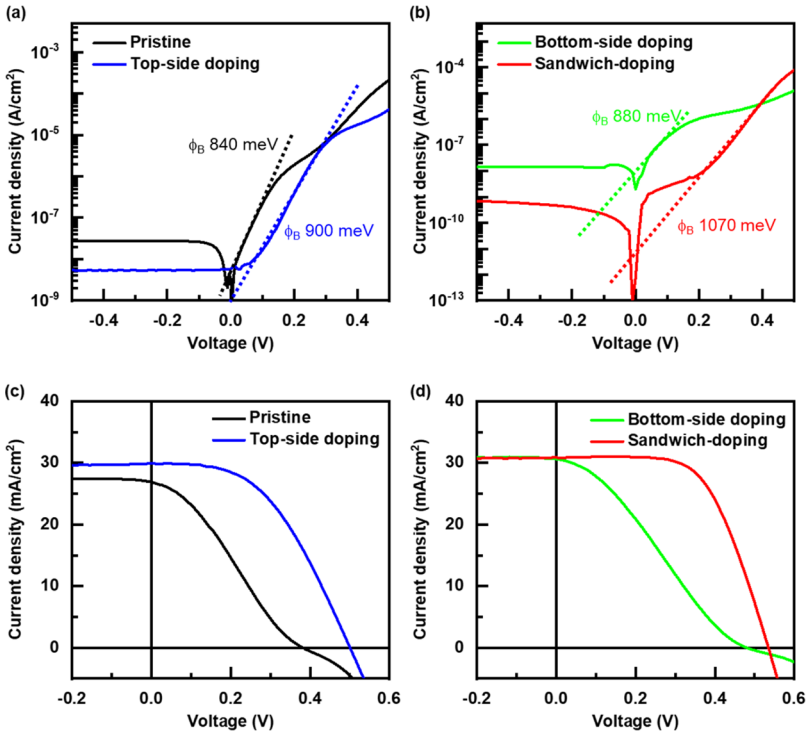

Figure 3. Characterization of graphene/silicon SJSCs fabricated by differently doped graphene. Dark $J-V$ curves of SJSCs with (a) pristine and top-side-doped graphene and (b) bottom-side-doped and sandwich-doped graphene. Light $J-V$ curves of SJSCs with (c) pristine and top-side-doped graphene and (d) bottom-side-doped and sandwich-doped graphene.

sandwich-doped graphene had PCE = 10.02% with a negligible change during 45 days under ambient conditions without any encapsulation.

RESULTS AND DISCUSSION

Graphene/silicon SJSCs with pristine, top-side-doped, bottom-side-doped, and sandwich-doped graphene (Figure 1a) were fabricated (Figures S1 and S2 in the Supporting Information). The top-side doping was performed by spin-coating a $HAuCl_4$ solution as a p-type dopant on the graphene surface.[26−28] In comparison, the bottom-side doping process involves simultaneous etching and doping without any postdoping or surface modification.[16,29,30] To achieve simultaneous etching and doping, a poly(methyl methacrylate) (PMMA)-coated graphene on a Cu foil was floated in ammonium persulfate (APS, etchant) solution that contained BI as a dopant. The BI adsorbed onto the bottom surface of graphene by $\pi-\pi$ interaction during the Cu etching process (Figure S2). After transfer to arbitrary substrates, the graphene exhibited p-doping characteristics without any additional doping process. Sandwich doping to maximize the p-doping effect was achieved by first doping the bottom side with graphene and then doping the top side with it.

X-ray photoelectron spectroscopy (XPS) analyses were performed to confirm the variation in atomic compositions of each type of doped graphene (Figures 1b, S3). The atomic composition was calculated by fitting each core-level spectrum, which was clearly related to the dopants that had been used (Figure 1b). The sandwich-doped graphene had the highest amount of dopant (atomic percentage): 1.11% Au 4f peak, 3.52% Cl 2p peak, and 6.22% N 1s; these results confirm successful p-doping on both sides of graphene. The work function of graphene was affected by three doping methods, confirmed by ultraviolet photoemission spectroscopy (UPS), as shown in Figure S4. The W_G of each type of graphene can be calculated as[27]

$$W_G = h\nu - (E_{cut\text{-}off} - E_F) \quad (1)$$

where $h\nu$ is the photon energy of the excitation light source (He I discharge lamp, 21.2 eV), $E_{cut\text{-}off}$ [eV] is the secondary electron cutoff energy, and E_f [eV] is the Fermi edge. The calculation indicated that pristine graphene had W_G = 4.46 eV, which is similar to a previous report.[31] The W_G values of top-side-doped, bottom-side-doped, and sandwich-doped graphene were calculated as 4.97, 4.82, and 5.07 eV, respectively (Figure 1c). Sandwich-doped graphene has the highest W_G owing to the combined p-doping effects of BI and $HAuCl_4$.[32]

To further investigate the doping effect on the graphene, Raman spectra were measured using a 514 nm laser (Figure 2a). The Raman shifts of the G-band and 2D-band depend on the degree of doping; the sandwich-doped graphene clearly showed a larger blue shift of G- and 2D-band (G-peak: from 1590 to 1600 cm^{-1}; 2D-peak: from 2701 to 2707 cm^{-1}) than other graphene samples owing to its heaviest p-doping effect. R_S of graphene was investigated using four-probe measurement. The R_S of pristine graphene was 471.2 Ω/sq (Figure 2b), which is similar to a previous report.[28] On the other hand, the R_S of sandwich-doped graphene was decreased to 165.4 Ω/sq, which shows that the doping increased the conductivity. In Figure 2c, the optical transmittances of the graphene samples between 400 and 1000 nm wavelength ranges are compared. At 550 nm, the pristine graphene had 96.4% of optical transmittance, top-side-doped had 94.4%, bottom-side-doped had 95.4%, and sandwich-doped had 93.1%; the changes show a negligible light absorption by the adsorbed dopants.[33] It is concluded that the sandwich-doping method rendered the

https://dx.doi.org/10.1021/acsomega.0c05871
ACS Omega 2021, 6, 3973−3979

graphene to have an increased work function at low R_S without significant loss of optical transmittance (>90%).

Dark $J-V$ curves of graphene/silicon SJSCs with different doping methods are displayed in Figure 3a,b.

$$J_s = J_0 \exp\left(-\frac{qV}{nkT} - 1\right) \quad (2)$$

where $q = 1.602 \times 10^{-19}$ eV is the absolute value of the electron charge, n is the ideality factor, $k = 8.62 \times 10^{-5}$ eV·K^{-1} is the Boltzmann constant, and $T = 298$ K. The calculated J_S value was considerably decreased from 5.24×10^{-9} A·cm^{-2} in pristine graphene to 9.31×10^{-12} A·cm^{-2} in sandwich-doped graphene; this reduction indicates that the charge-carrier recombination in sandwich-doped graphene/silicon SJSCs was significantly suppressed.[25]

Calculation used the nonideal diode model with charge carriers moving across over the ϕ_B by thermionic emission

$$J_0 = A^* T^2 \exp\left(-\frac{\phi_B}{kT}\right) \quad (3)$$

where J_0 [A·cm^{-2}] is the density of the reverse saturation current (i.e., the linear fitting to zero-bias voltage of the $J-V$ curve), $A^* = 112$ A·cm^{-2}·K^{-2} is the Richardson constant, $T = 298$ K is the temperature, and $k = 8.62 \times 10^{-5}$ eV·K^{-1} is the Boltzmann constant. The calculated ϕ_B of sandwich-doped graphene/silicon SJSC was 1070 meV, which was 230 meV higher than that of SJSC with pristine graphene. This difference indicates that the sandwich-doped graphene has wide band bending and an increased built-in electric field (V_{bi}),[34] as depicted in band diagrams of pristine and sandwich-doped SJSCs (Figure S5). Therefore, sandwich doping reduces charge-carrier recombination and thereby facilitates efficient charge-carrier separation and collection.

$J-V$ curves of graphene/silicon SJSCs were also measured under illumination of AM 1.5G (Figure 3c,d), and photovoltaic parameters (Table 1) were extracted. The cell that used

Table 1. Average and Standard Deviation ($n \geq 10$) Photovoltaic Parameters from Graphene/Silicon SJSCs

doping	V_{oc} (V)	J_{sc} (mA/cm^2)	FF (%)	PCE (%)
pristine	0.384 (±0.023)	26.88 (±0.58)	29.94 (±3.11)	2.998 (±0.107)
top-side doping	0.506 (±0.017)	29.92 (±2.67)	47.74 (±3.11)	7.142 (±0.188)
bottom-side doping	0.487 (±0.002)	30.29 (±2.06)	28.68 (±1.96)	4.229 (±0.748)
sandwich-doping	0.535 (±0.015)	30.86 (±2.43)	60.72 (±0.72)	10.02 (±1.142)

pristine graphene/silicon SJSC had short-circuit current density $J_{sc} = 26.88$ mA/cm^2, open-circuit voltage $V_{oc} = 0.384$ V, fill factor (FF) = 29.94%, and PCE = 2.998%. For the top-side-doped graphene/silicon SJSC, we tested different concentrations of the top-side dopant (Figure S6 and Table S1). The optimal concentration of 10 mM $HAuCl_4$ solution yielded $J_{sc} = 29.92$ mA/cm^2, $V_{oc} = 0.506$ V, FF = 47.74%, and PCE = 7.142%. All photovoltaic parameters were improved by the increase in ϕ_B as a result of top-side doping.

The bottom-side-doped graphene/silicon SJSC had $J_{sc} = 30.29$ mA/cm^2, $V_{oc} = 0.487$ V, FF = 28.68%, and PCE = 4.229%. This low FF was attributed to the high R_S of bottom-side-doped graphene. Various concentrations (1, 3, 6, 13, and 32 mM) of the BI dopant were tried for the sandwich doping process; then, the illuminated $J-V$ curves were measured (Figure S7 and Table S2). The SJSC doped with 1 mM BI had insufficient PCE = 7.385%. The SJSC doped with 32 mM BI had a poor PCE = 4.971% because the high concentration of BI dopants suppressed transport of photogenerated charge carriers and formed potential recombination centers to trap the free charge carriers.[35] The best performance of sandwich-doped SJSCs was obtained with 3 mM BI, which yielded $J_{sc} = 30.86$ mA/cm^2, $V_{oc} = 0.535$ V, FF = 60.72%, and PCE = 10.02% (334% greater than that of pristine graphene/silicon SJSC).

J_{sc} increased from 26.88 mA/cm^2 (pristine) to 30.86 mA/cm^2 (sandwich doping), and the same trend was also confirmed in external quantum efficiency (EQE) measurement (Figure S8); this increase could contribute to the increase in PCE enhancement slightly, but it was not sufficient to explain all of the dramatic improvement. Most of the improvement can be attributed to the combined effect of the increased V_{oc} and increased FF. The significant improvements in V_{oc} from 0.384 V (pristine) to 0.535 V (sandwich doping) originated from the increased ϕ_B, and the much increased FF was a result of the decreased series resistance from 497.96 Ω·cm^2 (pristine) to 92.55 Ω·cm^2 (sandwich doping). This was possible by the reduction of R_S of sandwich-doped graphene. The decreased series resistance facilitated charge-carrier transport and thus increased the resistance to charge-carrier recombination and thereby yielded an outstanding improvement in FF from 29.74% (pristine) to 60.72% (sandwich doping).

To confirm the long-term stability, we measured the $J-V$ curves over time on SJSC devices that had been stored under ambient conditions. Especially, we compared the photovoltaic parameters of the sandwich-doped SJSC to those of the top-side-doped SJSC (Figure 4a,b). V_{oc} and FF of the top-side-doped SJSC remarkably decreased over time, although J_{sc} remained unchanged; PCE decreased by 44.3% during storage for 45 days. However, the photovoltaic parameters of sandwich-doped SJSC were stable for 45 days, and its PCE did not change over the 45 days (Figure 4c). These phenomena can be explained by the variation of electrical properties with time. R_S of sandwich-doped graphene did not show a noticeable change, whereas that of top-side-doped graphene increased by about 159% after 45 days (Figure 4d).

To further investigate the long-term stability, we observed the compositional changes of Au^{3+}, Au^0, and the Cl atom in both top-side-doped and sandwich-doped graphene using XPS on the 1st and 45th days after doping (Figure S9 and Table S3). The doping stability of graphene doped by gold chloride was determined by measuring the change over time in the amounts of gold cations and chlorine anions.[36−38] The doping stability degraded due to aggregation of Au particles and desorption of Cl atoms.[39] In the top-side-doped graphene, the Au^{3+} $4f_{7/2}$ and Au^{3+} $4f_{5/2}$ peaks vanished, but the atomic composition of Au^0 increased from 0.52 to 0.95% owing to the aggregation of Au particles. The amount of Cl atoms decreased from 3.33 to 1.54% due to desorption of Cl atoms from the graphene surface. In contrast, in sandwich-doped graphene, the amounts of Au^{3+}, Au^0, and Cl atoms measured on the 45th day were similar to those measured on the 1st day. This stability indicates that the dopants were retained stably without degradation under ambient conditions.

We compared our stability results with previous reports[22−25] (Table 2). The SJSC with TETA-doped graphene had the

https://dx.doi.org/10.1021/acsomega.0c05871
ACS Omega 2021, 6, 3973−3979

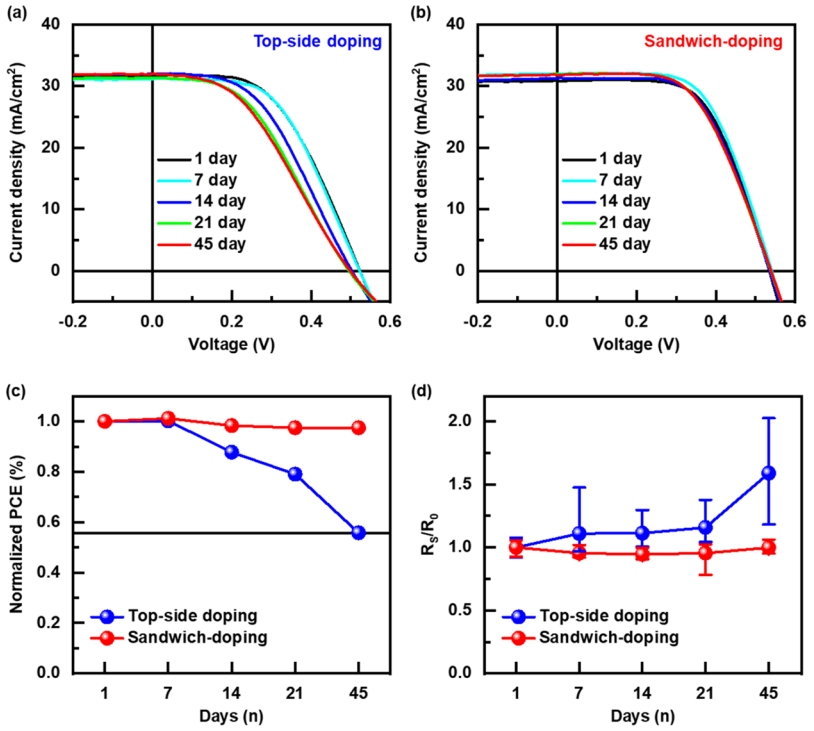

Figure 4. *J*−*V* curves of the cells with (a) top-side-doped graphene and (b) sandwich-doped graphene, measured on 1, 7, 14, 21, and 45 days after doping under ambient conditions. Change in (c) normalized PCE. (d) Ratio of sheet resistance R_s (after n day)/R_0 (1st day).

Table 2. Initial PCE and Reduced PCE of the Previously Reported Graphene/Silicon SJSCs in Comparison to Those of Our Study[a]

	solar cell culture	initial PCE (%)	reduced PCE (%)	days	ratio	year
1	*n*-Si/P3HT/graphene[23]	8.87	3.72	10	0.42	2017
2	*n*-Si/$SOCl_2$-doped graphene[22]	5.95	3.29	8	0.55	2013
3	*n*-Si/HNO_3-doped graphene/ARC[25]	14.1	6.47	20	0.46	2013
4	*n*-Si/TETA-doped graphene/PMMA[24]	5.48	5.37	10	0.98	2018
5	*n*-Si/$HAuCl_4$-doped graphene (top-side doping)	8.50	4.76	42	0.56	our work
6	*n*-Si/BI and $HAuCl_4$-doped graphene (sandwich doping)	10.02	9.75	42	0.97	our work

[a]Ratio = (reduced PCE)/(initial PCE).

highest retention of PCE (= reduced PCE/initial PCE), but the initial PCE was relatively low (5.48%) and the test period was relatively short (10 days). However, our SJSCs with sandwich-doped graphene had a much higher PCE (10.02%) and were stable for 45 days; this result suggests that the sandwich-doping method greatly improved the PCE and stability of SJSCs without encapsulation.

CONCLUSIONS

We have demonstrated how three doping methods affected the work function and electrical properties of graphene. The sandwich-doping method with the BI bottom dopant and $HAuCl_4$ top dopant achieved strongly p-doped graphene with high stability. The work function of sandwich-doped graphene increased to 5.07 eV, which is 0.61 eV higher than that of pristine graphene. The R_S of sandwich-doped graphene was 165.4 Ω/sq, which is 35.1% lower than that of pristine graphene. Therefore, the SJSC with sandwich-doped graphene had a much higher FF and V_{oc} and an increased PCE of 10.02%, which is 334% higher than that of pristine graphene. In addition, the sandwich-doped SJSC maintained its initial PCE for 45 days under ambient conditions without noticeable degradation. We believe that our study provides a promising doping method for graphene-based optoelectronics.

EXPERIMENTAL SECTION

Graphene Synthesis and Transfer. A monolayer of graphene was grown on a 25 μm-thick copper (Cu) foil by chemical vapor deposition (CVD). The Cu foil was loaded into the chamber; then, its temperature was elevated to 1000 °C under H_2 (100 sccm) gas. The graphene was synthesized with flowing CH_4 (125 sccm) and H_2 (100 sccm) for 30 min at 1000 °C. The chamber was then cooled to room temperature, and the Cu foil was removed from the chamber. A protective layer of poly(methyl methacrylate) (PMMA) was spin-coated on the one side of the graphene, while it was still attached to the Cu foil. The back side of the graphene was removed using oxygen plasma (100 W, 12 S, 160 mTorr). The underlying Cu foil was etched in 0.175 M ammonium persulfate ($(NH_4)_2S_2O_8$, APS) solution. The final graphene was rinsed in deionized water (DIW) and transferred to the target substrate. Bilayer graphene was made by repeating the transfer process.

https://dx.doi.org/10.1021/acsomega.0c05871
ACS Omega 2021, 6, 3973−3979

Fabrication of Schottky Junction Solar Cells. A 1.5 cm × 1.5 cm piece of n-type silicon wafer (10−30 Ω·cm, 500 μm thickness, oriented along the [100] plane) with a 300 nm SiO_2 layer was patterned by photolithography (MDA-400S, MIDAS) in the middle of the substrate. The oxide layer was wet-etched by buffered oxide etching (BOE) solution to expose n-type Si. The rinsed graphene layer was transferred to the target substrate and then annealed at 80 °C to improve graphene adhesion onto the substrate. The samples were soaked in acetone solution at 80 °C for 30 min to remove the PMMA layer. An indium−gallium (In−Ga) eutectic (≥99.99%, Sigma-Aldrich) was used as a back electrode, and gold (Au) was deposited by evaporation as a front electrode. For top-side doping, the graphene on the substrate was spin-casted with $HAuCl_4$ (10 mM in nitromethane) at 2500 rpm for 1 min. For sandwich doping, 3 mM BI was added into APS solution to dope the graphene, while the Cu foil was being etched away. The graphene was transferred to the target substrate; then, $HAuCl_4$ (10 mM in nitromethane) solution was cast on the graphene to achieve top-side doping.

Characterization. The solar cell was measured using a Keithley 2400 source meter and a Xenon lamp (AM 1.5G illumination, 100 $mW{\cdot}cm^{-2}$). The active area was 0.4 cm^2. The external quantum efficiency (EQE) was measured using an EQE system (Oriel IQE-200, New port). To characterize the graphene doping state, Raman spectroscopy (Horiba) analysis was performed using a 514-nm laser. Transmittance of graphene was characterized using a UV−Vis−NIR (Jasco, V-670) spectrophotometer. X-ray photoelectron spectroscopy (XPS, Thermo-Scientific) was performed using monochromatic Al Kα X-ray photons ($h\nu$ = 1486.6 eV). The work function of graphene was measured using ultraviolet photoelectron spectroscopy (UPS) with He I radiation (21.2 eV). R_s (5 cm × 5 cm graphene transferred onto the SiO_2 substrate) was measured using a four-point probe (Dasol ENG).

■ ASSOCIATED CONTENT

Supporting Information

The Supporting Information is available free of charge at https://pubs.acs.org/doi/10.1021/acsomega.0c05871.

Fabrication process and further analysis of four differently doped graphene films and the $J-V$ curve characterization of graphene/silicon Schottky junction solar cells depending on the concentration of dopants (PDF)

■ AUTHOR INFORMATION

Corresponding Authors

Gun Young Jung − *School of Materials Science and Engineering, Gwangju Institute of Science and Technology (GIST), Gwangju 61005, Republic of Korea;* orcid.org/0000-0003-1163-8651; Email: gyjung@gist.ac.kr

Sukang Bae − *Functional Composite Materials Research Center, Korea Institute of Science and Technology, Jeonbuk 55324, Republic of Korea;* orcid.org/0000-0002-3019-0584; Email: sbae@kist.re.kr

Authors

Min Ji Im − *Functional Composite Materials Research Center, Korea Institute of Science and Technology, Jeonbuk 55324, Republic of Korea; School of Materials Science and Engineering, Gwangju Institute of Science and Technology (GIST), Gwangju 61005, Republic of Korea*

Seok-Ki Hyeong − *Functional Composite Materials Research Center, Korea Institute of Science and Technology, Jeonbuk 55324, Republic of Korea*

Min Park − *Functional Composite Materials Research Center, Korea Institute of Science and Technology, Jeonbuk 55324, Republic of Korea*

Seoung-Ki Lee − *Functional Composite Materials Research Center, Korea Institute of Science and Technology, Jeonbuk 55324, Republic of Korea;* orcid.org/0000-0002-8786-0251

Tae-Wook Kim − *Department of Flexible and Printable Electronics, Jeonbuk National University, Jeonbuk 54896, Republic of Korea;* orcid.org/0000-0003-2157-732X

Complete contact information is available at: https://pubs.acs.org/10.1021/acsomega.0c05871

Notes

The authors declare no competing financial interest.

■ ACKNOWLEDGMENTS

This work was supported by the National Research Council of Science & Technology (NST) grant by the Korea government (MSIT) (no. CRC-20-01-NFRI). M.J.I. thanks Da Bin Son in INCHEON TECHNOPARK and Dr. Sung Bum Kang at UIUC. G.Y.J. was partially supported by the Basic Science Research Program (NRF-2019R1A2B5B01070640) of the National Research Foundation of Korea funded by the Ministry Science and ICT.

■ REFERENCES

(1) Yoshikawa, K.; Kawasaki, H.; Yoshida, W.; Irie, T.; Konishi, K.; Nakano, K.; Uto, T.; Adachi, D.; Kanematsu, M.; Uzu, H.; Yamamoto, K. Silicon Heterojunction Solar Cell with Interdigitated Back Contacts for a Photoconversion Efficiency over 26%. *Nat. Energy* **2017**, *2*, 17032.

(2) Makino, T.; Tanimoto, S.; Hayashi, Y.; Kato, H.; Tokuda, N.; Ogura, M.; Takeuchi, D.; Oyama, K.; Ohashi, H.; Okushi, H.; Yamasaki, S. Diamond Schottky-pn Diode with High Forward Current Density and Fast Switching Operation. *Appl. Phys. Lett.* **2009**, *94*, 262101−262103.

(3) Baliga, B. J. The pinch rectifier: A low-forward-drop high-speed power diode. *IEEE Electron Device Lett.* **1984**, *5*, 194−196.

(4) Anderson, W. A.; Delahoy, A. E.; Milano, R. A. An 8% Efficient Layered Schottky-Barrier Solar Cell. *J. Appl. Phys.* **1974**, *45*, 3913−3915.

(5) Jäckle, S.; Mattiza, M.; Liebhaber, M.; Bronstrup, G.; Rommel, M.; Lips, K.; Christiansen, S. Junction Formation and Current Transport Mechanisms in Hybrid n-Si/PEDOT: PSS Solar Cells. *Sci. Rep.* **2015**, *5*, 13008.

(6) Jeong, H.; Song, H.; Pak, Y.; Kwon, I. K.; Jo, K.; Lee, H.; Jung, G. Y. Enhanced Light Absorption of Silicon Nanotube Arrays for Organic/Inorganic Hybrid Solar Cells. *Adv. Mater.* **2014**, *26*, 3445−3450.

(7) Canali, C.; Cantellani, F.; Mantovani, S.; Prudenziati, M. Thin Pt and Pd Silicide Schottky Barriers for Silicon Solar Cells. *J. Phys. D: Appl. Phys.* **1977**, *10*, 2481−2489.

(8) Gerling, L. G.; Mahato, S.; Morales-Vilches, A.; Masmitja, G.; Ortega, P.; Voz, C.; Alcubilla, R.; Puigdollers, J. Transition Metal Oxides as Hole-Selective Contacts in Silicon Heterojunctions Solar Cells. *Sol. Energy Mater. Sol. Cells* **2016**, *145*, 109−115.

(9) Ghosh, A. K.; Fishman, C.; Feng, T. SnO2/Si solar cells-heterostructure or Schottky-barrier or MIS-type device. *J. Appl. Phys.* **1978**, *49*, 3490−3498.

(10) Kang, S. B.; Kwon, K. C.; Choi, K. S.; Lee, R.; Hong, K.; Suh, J. M.; Im, M. J.; Sanger, A.; Choi, I. Y.; Kim, S. Y.; Shin, J. C.; Jang, H. W.; Choi, K. J. Transfer of Ultrathin Molybdenum Disulfide and Transparent Nanomesh Electrode onto Silicon for Efficient Heterojunction Solar Cells. *Nano Energy* **2018**, *50*, 649−658.
(11) Akama, T.; Okita, W.; Nagai, R.; Li, C.; Kaneko, T.; Kato, T. Schottky Solar Cell using Few-Layered Transition Metal Dichalcogenides toward Large-Scale Fabrication of Semitransparent and Flexible Power Generator. *Sci. Rep.* **2017**, *7*, 11967.
(12) Pradhan, S. K.; Xiao, B.; Pradhan, A. K. Enhanced photoresponse in p-Si/MoS2 heterojunction-based solar cells. *Sol. Energy Mater. Sol. Cells* **2016**, *144*, 117−127.
(13) Bae, S.; Kim, H.; Lee, Y.; Xu, X.; Park, J.-S.; Zheng, Y.; Balakrishnan, J.; Lei, T.; Ri Kim, H.; Song, Y. I.; Kim, Y.-J.; Kim, K. S.; Özyilmaz, B.; Ahn, J.-H.; Hong, B. H.; Iijima, S. Roll-to-roll Production of 30-inch Graphene Films for Transparent Electrodes. *Nat. Nanotechnol.* **2010**, *5*, 574−578.
(14) Lee, C. K.; Seo, J. G.; Kim, H. J.; Hong, S. J.; Song, G.; Ahn, C.; Lee, D. J.; Song, S. H. Versatile and Tunable Electrical Properties of Doped Nonoxidized Graphene Using Alkali Metal Chlorides. *ACS Appl. Mater. Interfaces* **2019**, *11*, 42520−42527.
(15) Park, J.; Lee, W. H.; Huh, S.; Sim, S. H.; Kim, S. B.; Cho, K.; Hong, B. H.; Kim, K. S. Work-Function Engineering of Graphene Electrodes by Self-Assembled Monolayers for High-Performance Organic Field-Effect Transistors. *J. Phys. Chem. Lett.* **2011**, *2*, 841−845.
(16) Koo, D.; Jung, S.; Seo, J.; Jeong, G.; Choi, Y.; Lee, J.; Lee, S. M.; Cho, Y.; Jeong, M.; Lee, J.; Oh, J.; Yang, C.; Park, H. Flexible Organic Solar Cells Over 15% Efficiency with Polyimide-Integrated Graphene Electrodes. *Joule* **2020**, *4*, 1021−1034.
(17) Høiaas, I. M.; Mulyo, A. L.; Vullum, P. E.; Kim, D.-C.; Ahtapodov, L.; Fimland, B.-O.; Kishino, K.; Weman, H. GaN/AlGaN Nanocolumn Ultraviolet Light-Emitting Diode using Double-Layer Graphene as Substrate and Transparent Electrode. *Nano Lett.* **2019**, *19*, 1649−1658.
(18) Aïssa, B.; Nedil, M.; Kroeger, J.; Ali, A.; Isaifan, R. J.; Essehli, R.; Mahmoud, K. A. Graphene Nanoplatelet Doping of P3HT:PCBM Photoactive Layer of Bulk Heterojunction Organic Solar Cells for Enhancing Performance. *Nanotechnology* **2018**, *29*, 105405.
(19) Yang, N.; Zhai, J.; Wang, D.; Chen, Y.; Jiang, L. Two-Dimensional Graphene Bridges Enhanced Photoinduced Charge Transport in Dye-Sensitized Solar Cells. *ACS Nano* **2010**, *4*, 887−894.
(20) Tong, S. W.; Wang, Y.; Zheng, Y.; Ng, M.-F.; Loh, K. P. Graphene Intermediate Layer in Tandem Organic Photovoltaic Cells. *Adv. Funct. Mater.* **2011**, *21*, 4430−4435.
(21) Li, X.; Zhu, H.; Wang, K.; Cao, A.; Wei, J.; Li, C.; Jia, Y.; Li, Z.; Li, X.; Wu, D. Graphene-on-Silicon Schottky Junction Solar Cells. *Adv. Mater.* **2010**, *22*, 2743−2748.
(22) Cui, T.; Lv, R.; Huang, Z.-H.; Chen, S.; Zhang, Z.; Gan, X.; Jia, Y.; Li, X.; Wang, K.; Wu, D.; Kang, F. Enhanced Efficiency of Graphene/Silicon Heterojunction Solar Cells by Molecular Doping. *J. Mater. Chem. A* **2013**, *1*, 5736−5740.
(23) Xu, D.; He, J.; Yu, X.; Gao, D.; Ma, L.; Mu, X.; Zhong, M.; Xu, Y.; Ye, J.; Xu, M.; Yang, D. Illumination-Induced Hole Doping for Performance Improvement of Graphene/n-Silicon Solar Cells with P3HT Interlayer. *Adv. Electron. Mater.* **2017**, *3*, 1600516.
(24) Shin, D. H.; Jang, C. W.; Lee, H. S.; Seo, S. W.; Kim, S.; Choi, S.-H. Graphene/Si Solar Cells Employing Triethylenetetramine Dopant and Polymethylmethacrylate Antireflection Layer. *Appl. Surf. Sci.* **2018**, *433*, 181−187.
(25) Shi, E.; Li, H.; Yang, L.; Zhang, L.; Li, Z.; Li, P.; Shang, Y.; Wu, S.; Li, X.; Wei, J.; Wang, K.; Zhu, H.; Wu, D.; Fang, Y.; Cao, A. Colloidal Antireflection Coating Improves Graphene-Silicon Solar Cells. *Nano Lett.* **2013**, *13*, 1776−1781.
(26) Garg, R.; Dutta, N.; Choudhury, N. Work Function Engineering of Graphene. *Nanomaterials* **2014**, *4*, 267−300.
(27) Syu, J.-Y.; Chen, Y.-M.; Xu, K.-X.; He, S.-M.; Hung, W.-C.; Chang, C.-L.; Su, C.-Y. Wide-Range Work-Function Tuning of Active Graphene Transparent Electrodes via Hole Doping. *RSC Adv.* **2016**, *6*, 32746−32756.
(28) Kim, K. K.; Reina, A.; Shi, Y.; Park, H.; Li, L. J.; Lee, Y. H.; Kong, J. Enhancing the Conductivity of Transparent Graphene Films via Doping. *Nanotechnology* **2010**, *21*, 1−6.
(29) Kim, S. J.; Ryu, J.; Son, S.; Yoo, J. M.; Park, J. B.; Won, D.; Lee, E.-K.; Cho, S.-P.; Bae, S.; Cho, S.; Hong, B. H. Simultaneous Etching and Doping by Cu-Stabilizing Agent for High-Performance Graphene-Based Transparent Electrodes. *Chem. Mater.* **2014**, *26*, 2332−2336.
(30) Jo, K.; Kim, S.-M.; Lee, S.-M.; Kim, J.-H.; Lee, H.-J.; Kim, K. S.; Kwon, Y. D.; Kim, K.-S. One-Step Etching, Doping, and Adhesion-Control Process for Graphene Electrodes. *Carbon* **2015**, *82*, 168−175.
(31) Liu, Q.; Gong, Y.; Wang, T.; Chan, W.-L.; Wu, J. Metal-Catalyst-Free and Controllable Growth of High-Quality Monolayer and AB-Stacked Bilayer Graphene on Silicon Dioxide. *Carbon* **2016**, *96*, 203−211.
(32) Kim, Y.; Park, J.; Kang, J.; Yoo, J. M.; Choi, K.; Kim, E. S.; Choi, J.-B.; Hwang, C.; Novoselov, K. S.; Hong, B. H. A Highly Conducting Graphene Film with Dual-side Molecular n-doping. *Nanoscale* **2014**, *6*, 9545−9549.
(33) Adhikari, S.; Perello, D. J.; Biswas, C.; Ghosh, A.; Luan, N. V.; Park, J.; Yao, F.; Rotkin, S. V.; Lee, Y. H. Determining the Fermi Level by Absorption Quenching of Monolayer Graphene by Charge Transfer Doping. *Nanoscale* **2016**, *8*, 18710−18717.
(34) Liu, X.; Zhang, X. W.; Meng, J. H.; Yin, Z. G.; Zhang, L. Q.; Wang, H. L.; Wu, J. L. High Efficiency Schottky Junction Solar Cells by Co-Doping of Graphene with Gold Nanoparticles and Nitric Acid. *Appl. Phys. Lett.* **2015**, *106*, 233901−233905.
(35) Ding, K.; Zhang, X.; Xia, F.; Whang, R.; Kuang, Y.; Duhm, S.; Jie, J.; Zhang, X. Surface Charge Transfer Doping Induced Inversion Layer for High Performance Graphene/Silicon Heterojunction Solar Cells. *J. Mater. Chem. A* **2017**, *5*, 285−291.
(36) Kwon, K. C.; Kim, B. J.; Lee, J.-L.; Kim, S. Y. Role of Ionic Chlorine in the Thermal Degradation of Metal Chloride-Doped Graphene Sheets. *J. Mater. Chem. C* **2013**, *1*, 253−259.
(37) Abdullah-Al-Galib, M.; Hou, B.; Shahriad, T.; Zivanovic, S.; Radadia, A. D. Stability of Few Layer Graphene Films Doped with Gold (III) Chloride. *Appl. Surf. Sci.* **2016**, *366*, 78−84.
(38) Kim, S. M.; Kim, K. K.; Jo, Y. W.; Park, M. H.; Chae, S. J.; Duong, D. L.; Yang, C. W.; Kong, J.; Lee, Y. H. Role of Anions in the AuCl3-Doping of Carbon Nanotubes. *ACS Nano* **2011**, *5*, 1236−1242.
(39) Kwon, K. C.; Kim, B. J.; Lee, J.-L.; Kim, S. Y. Effect of Anions in Au Complexes on Doping and Degradation of Graphene. *J. Mater. Chem. C* **2013**, *1*, 2463−2469.

https://dx.doi.org/10.1021/acsomega.0c05871
ACS Omega 2021, 6, 3973−3979